Available online at www.sciencedirect.com

jmr&t Journal of Materials Research and Technology

www.jmrt.com.br

Original Article

Corrosion behavior of Al6061 alloy weldment produced by friction stir welding process

Farhad Gharavi[a], *Khamirul Amin Matori*[a,b,*], *Robiah Yunus*[a], *Norinsan Kamil Othman*[c], *Firouz Fadaeifard*[a]

[a] *Materials Synthesis and Characterization Laboratory, Institute of Advanced Technology, Universiti Putra Malaysia, Serdang, Malaysia*

[b] *Department of Physics, Faculty of Science, Universiti Putra Malaysia, Serdang, Malaysia*

[c] *Schools of Applied Physics, Faculty of Science and Technology, University Kebangsaan Malaysia, Bangi, Malaysia*

ARTICLE INFO

Article history:
Received 16 July 2014
Accepted 29 January 2015
Available online 13 March 2015

Keywords:
Friction stir welding
Aluminum alloy
Pitting corrosion
Microstructure
Intermetallic particles

ABSTRACT

In this work, the corrosion behavior of welded lap joints of AA6061-T6 aluminum alloy produced by friction stir welding process has been investigated. Corrosion properties of welded lap joints were studied by cyclic polarization and electrochemical impedance spectroscopy tests. All tests were performed in an aerated 0.6 mol L^{-1} NaCl aqueous solution with pH = 6.5 at a temperature of 30 °C to characterize corrosion morphology and realize corrosion features of weld regions as opposed to the parent alloy. The microstructure of weld nugget (WN), heated affected zone (HAZ), and parent alloy were analyzed using scanning electron microscopy and energy dispersive spectroscopy. The experimental results indicated that the welding process has a major effect on the corrosion resistance, which possibly associated to the break-down and dissolution of intermetallic particles. It is supposed that an increasing in intermetallic distributed throughout the matrix of weld regions increases the galvanic corrosion couples. Furthermore, by decreasing the grain size in the weld regions, the susceptibility to corrosion is enhanced. The pitting corrosion and intergranular attack are the dominant corrosion types in the weld regions and the parent alloy.

1. Introduction

Aluminum 6061 is a typical alloy of 6xxx series and includes Al–Mg–Si alloying elements. The high amount of alloying elements added to increase the strength lead to the formation of large intermetallic precipitates during casting. These precipitates are too large to be greatly affected by subsequent thermomechanical processing [1]. Many reports have demonstrated that coarse intermetallic precipitates influence the corrosion behavior of aluminum alloys [2–4]. The presence of these precipitates in the microstructure could

* *Corresponding author.*
E-mail: khamirul@upm.edu.my (K.A. Matori).

http://dx.doi.org/10.1016/j.jmrt.2015.01.007

Table 1 – Nominal composition of parent alloy used in the welding process (in wt%).

Alloy	Al	Si	Fe	Cu	Mn	Mg	Cr	Ti	Zn
Al6061	Bal	0.66	0.30	0.27	0.03	1.00	0.18	0.02	0.05

significantly diminish a material's resistance to localized corrosion. The corrosion behavior of intermetallic precipitates depends mainly upon their redox potential with respect to the matrix. Intermetallic precipitates more noble than the matrix serve as cathodes; therefore, the surrounding matrix experiences anodic dissolution, and localized corrosion would subsequently progress [1]. As a part of the fabrication process, welding is one of the most important manufacturing technologies used in the aluminum alloy industry. In fact, the main problem associated with this kind of joint process can arise from the focus on heat-treatable alloys. Accordingly, heat generated by the welding process, can change the microstructure of aluminum alloy and chemistry as well as dimension and distribution of the intermetallic particles in the matrix of aluminum alloy. Thus, the welded joints of aluminum alloy have different localized corrosion behavior in an aggressive medium.

From the view point of localized corrosion, the most important feature of alloy microstructures is the distribution of intermetallic particles [3]. In general, some of the intermetallic particles will show different electrochemical characteristics as opposed to the behavior of the matrix. This difference gives rise to susceptibility to localized form of corrosion. In this case, some intermetallic particles may be either anodic or cathodic reactive to the alloy matrix. Cathodic reactive leads to alloy matrix dissolution, anodic reactive leads to dissolve preferentially [5]. The corrosion behavior of the FSW in different aluminum alloys has been examined by a number of authors so that the most investigations of corrosion behavior are performed on butt joints, while other configuration joints such as T-joint and lap joint are rarely considered [4–16]. The corrosion of aluminum alloy friction stir welds is commonly investigated using methods such as immersion test, polarization techniques, electrochemical impedance spectroscopy (EIS), stress corrosion cracking (SCC) test, and cyclic spray tests. Meanwhile, those experimental cyclic polarization and electrochemical impedance spectroscopy (EIS) tests are scarcely reported [9]. The aim of this research is to evaluate the localized corrosion behavior of friction lap welded joints of AA6061-T6 in 0.6 mol L^{-1} NaCl solution by means of cyclic polarization (pitting scan) and electrochemical impedance spectroscopy tests.

2. Experimental procedure

2.1. Materials and welding parameters

Friction stir welding technique by applying automatic CNC machine was used to produce lap welds. The parent alloy used was AA6061-T6 aluminum plates with thickness of 5 mm. The nominal compositions (in wt%) is displayed in Table 1. The lap joint configuration was prepared to produce the joints. The direction of welding was normal to the rolling direction of aluminum plates. A non-consumable welding tool made of high carbon steel (H13) was applied to fabricate the joints. The welding conditions and the chosen tool parameters used for welding in this work used to produce the joints in this investigation are listed in Table 2. To improve the weld joining, the tool was tilted 3° from the plate's normal direction toward the trailing side of the tool during welding.

Table 2 – Welding conditions and process parameters used in this work.

Parameter	Value
Rotation speed (rpm)	900
Welding speed (mm/min)	40
Tool shoulder diameter (mm)	20
Pin diameter (mm)	8
Pin length (mm)	8
Tilt angle (°)	3
Pin profile	Coniformed and left hand thread of 1 mm pitch

2.2. Electrochemical measurements

Electrochemical measuring was carried out with a conventional three-electrode-electrochemical glass cell using an EG&G Princeton Applied Research 2273 Potentiostat controlled by softcorr 352. The cell was open to the air and the measurements were conducted at a temperature of 30 °C. Each set of working electrodes, which were the WNZ (weld nugget zone), HAZ (heat affected zone), and parent alloy (PA) specimens, was connected to a copper wire, and sealed with epoxy resin with the exposure area of 1 cm^2 for the PA and 0.8 cm^2 for the WNZ as well as 0.3 cm^2 for the HAZ. A graphite rod and a saturated calomel electrode (SCE) were served as counter and reference electrodes, respectively. The test solution was a stagnant aerated 0.6 mol L^{-1} NaCl aqueous solution with pH = 6.5 at a temperature of 30 °C. The exposed surface of each specimen was ground using abrasive SiC papers through 600-grade to 1200-grade, and were mechanically polished with 1 μm diamond paste, rinsed with double distilled water, and degreased with ethanol. The degreased working electrodes were then dipped in concentrated HNO_3 for 30 s. After that, they were rinsed with deionized water and inserted into NaCl solution.

The cyclic polarization of specimens, after 30 min of immersion in the electrolyte, were performed by starting scanning electrode potential from an initial potential of −0.25 V below the OCP up to −0.2 V. The scan direction then was reversed and the potentials were scanned back to the initial potential. A vertex current density of 0.001 A/cm^2 was applied. From cyclic polarization, various corrosion parameters such as corrosion potential (E_{corr}), pitting potential (E_{pit}), repassivation/protection (E_{prot}) potential, and pit transition potential (E_{ptp}) were obtained.

In addition, electrochemical impedance spectroscopy (EIS) experiments were carried out at OCP over a frequency ranging

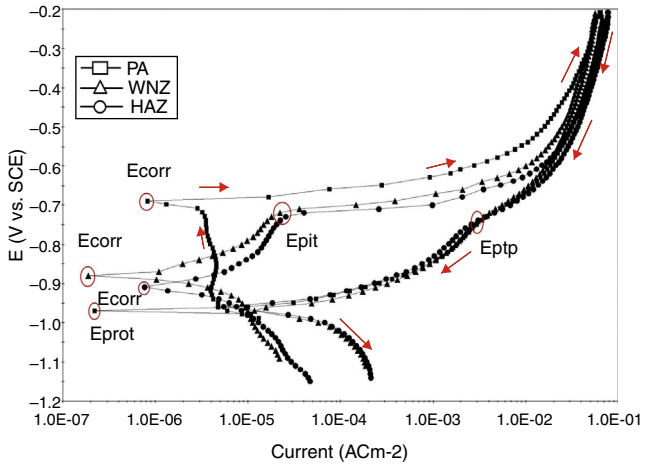

Fig. 1 – Cyclic polarization curves of the parent alloy and weld regions in 0.6 mol L^{-1} with pH = 6.5 at 30 °C.

from 100 kHz to 10 mHz, and AC 10 mV amplitude was superimposed on this test. The Zsim win 3.21 software was used for data modeling of the equivalent circuit proposed.

2.3. *Microstructure evaluation*

Microstructural examination of AA6061-T6 welded lap joints before and after corrosion tests was analyzed by scanning electron microscopy (SEM), energy dispersive spectroscopy (EDS), and atomic force microscopy (AFM) techniques.

3. Results and discussion

3.1. *Electrochemical behavior*

Cyclic polarization plots obtained for the parent alloy and weld regions in contact with 0.6 mol L^{-1} NaCl solution having near natural pH are shown in Fig. 1. The average values of potential are summarized in Table 3. From this table, it is evidence that the almost similar values of E_{pit} for the WNZ and HAZ regions of welded lap joints in test solution may indicate that the onset of pitting is mainly determined by Cl^- ion concentration and not by O_2 content [17]. According to Fig. 2, it is obvious that the cyclic plots of parent alloy and each region of welded lap joint show an example of negative hysteresis, with pitting potential located at the same position of that of corrosion potential, repassivation potential (E_{rp}) less than E_{corr}, and narrow area of the hysteresis loop, suggesting no nucleation and growth of pitting during the reverse scan [17,18]. The lower hysteresis in the presence of oxygen is due to repassivation assisted by O_2 reduction on constituent particles sites, indicating that not all such species has been consumed in accelerating pitting corrosion. Moreover, the protection potential of the WNZ and HAZ regions is more negative than the pitting potential. This means that the WNZ and HAZ regions did not show more tendencies to pitting corrosion. The cyclic polarization curves show a small region of passivity with the current density practically dependent on applied potential up to pitting potential $E_{pit} = -0.730$ mV. Then, the current density increase abruptly until it reaches a certain value; after that, it continues to increase slightly with increasing potential. Reverse polarization curve showed a negative hysteresis, suggesting no pitting is expected.

Furthermore, it is clear that the repassivation potential (E_{rp}) or the protection potential (E_{prot}) is less than E_{corr} in lap welded joints. It is well established that the size of the pitting loop is a rough indication of pitting tendency [17–20], so, the loop created in cyclic polarization plots shows the smallest tendency to pitting corrosion. In this case, the loop-like passivity could be related to traces of oxygen reduction at the already reactive joint surface. Hysteresis is produced upon scan reversal, and there is no intersecting the forward scan in the passive current region at E_{prot}. Narrower hysteresis and, consequently, more negative E_{prot}, are obtained for welded lap joints. Indeed, a potential step in the reverse scan, the so-called pit transition potential (E_{ptp}), is detected for lap welded joints. Additionally, E_{ptp} occurrence with different abruptness at the step (change of slope) is obtained for welded lap joints [17–20]. This indicates that the hysteresis features of cyclic polarization depend on the nature of the parent alloy and welding parameters under the present experimental conditions. In this respect, it is clear that the change of slope is sharper in all joints. This behavior shows that the tendency of all joints to repassivation

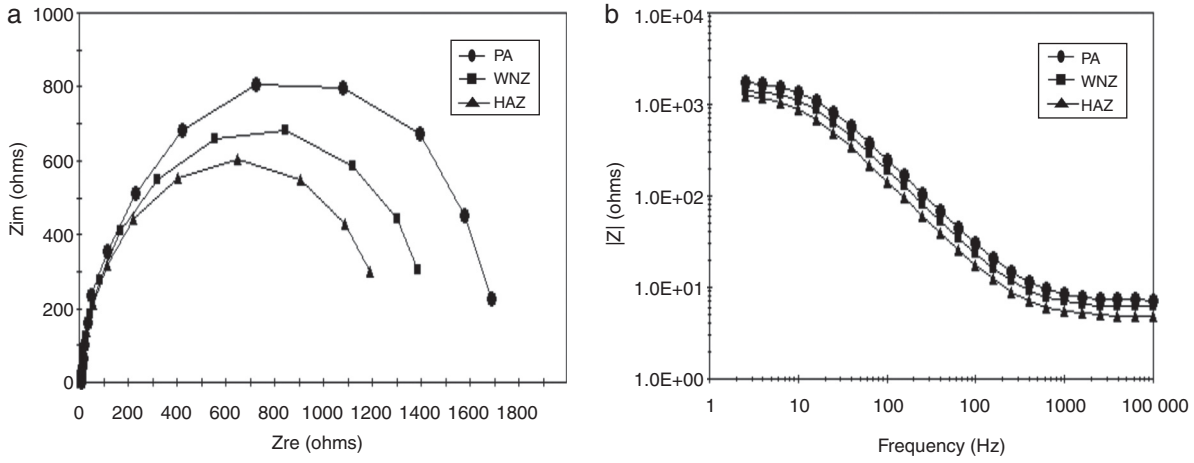

Fig. 2 – Typical impedance plots (a) Nyquist, (b) Bode for parent alloy and weld regions in 0.6 mol L^{-1} with pH = 6.5 at 30 °C.

Table 3 – Average characteristic potential (mV vs. SCE), corrosion current density, and corrosion rate of parent alloy and welded lap joint from pitting scans.

Material/process	E_{corr}	E_{pit}	E_{ptp}	E_{prot}	I_{corr} ($\mu A/cm^{-2}$)	C.R MPY)
Parent alloy	−698	−698	−745	−980	0.76	0.415
FSLW joint-WNZ	−865	−730	−749	−954	2.35	1.02
FSLW joint-HAZ	−908	−733	−750	−955	3.73	1.31

is the highest. The remarkable features of the reverse scan among the welded joints, allow the qualitative discrimination of the localized corrosion behavior. Analysis of the hysteresis loop and the corresponding shift in E_{prot}, indicate that the amount of pit propagation with consequent difficulty for complete surface repassivation is increased to near the corrosion potential. Thus, the welded joint shows the better susceptibility to pitting corrosion. According to these results, the significance of E_{prot} is almost misleading, not allowing discrimination between pitting corrosion and other possible forms of localized corrosion with more restricted conditions, such as intergranular corrosion (IGC).

The impedance diagrams for the parent alloy and the different weld regions including the WNZ and HAZ in an aerated 0.6 mol L^{-1} NaCl aqueous solution with pH = 6.5 a temperature of 30 °C after 0.5 h immersion are shown in Fig. 2. The various corrosion parameters obtained by fitting the equivalent circuit are listed in Table 4. From these results, it can be found that the oxide layers of aluminum alloy are composed of two parts. Upon exposure of aluminum to air, the aluminum oxide is formed on its surface, and after exposure to aqueous solution, another layer is, also, formed on its surface. This layer is generally caused by the hydration of aluminum. The frequency power values indicate that the inner layer is

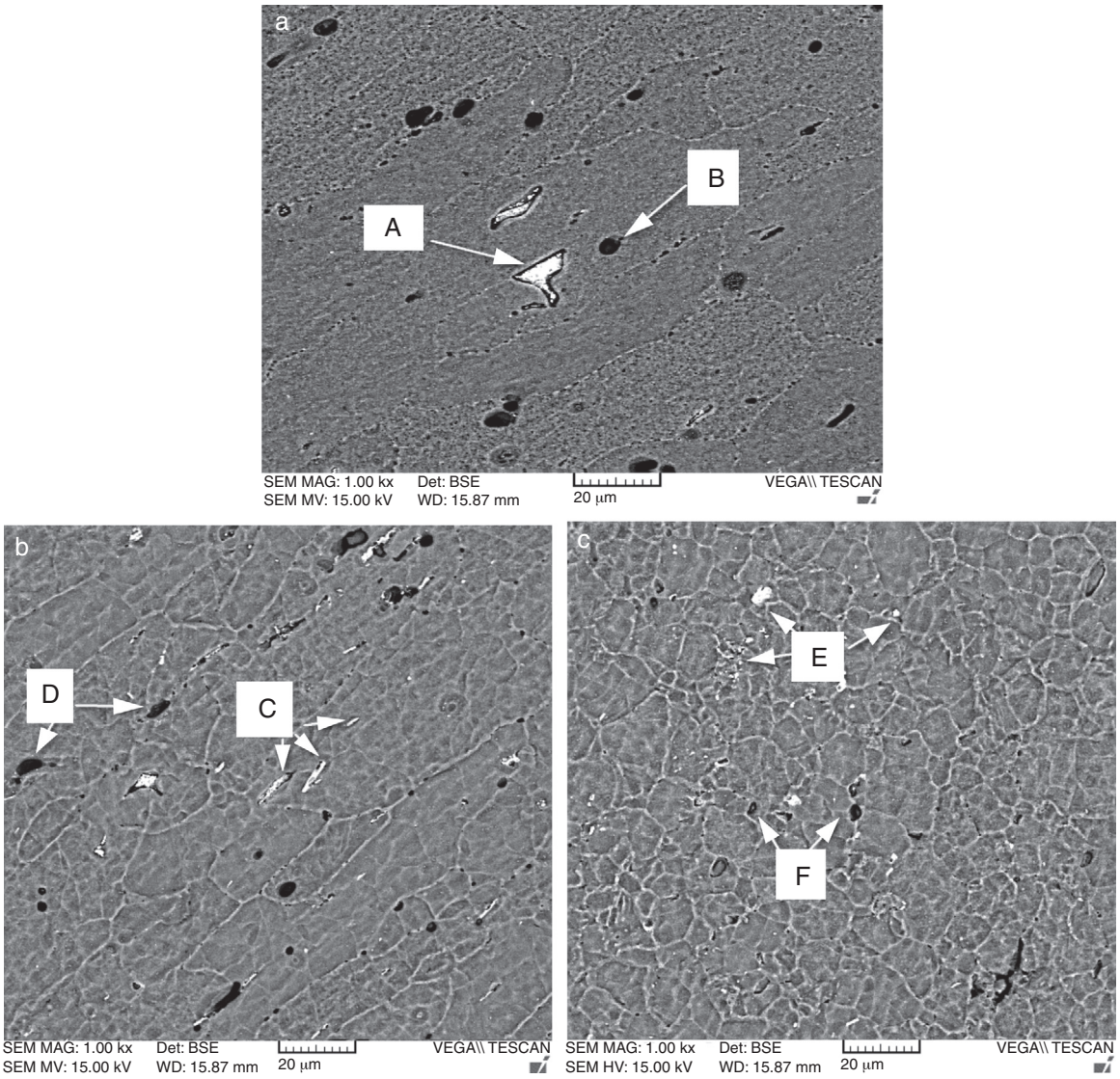

Fig. 3 – BSE micrograph of (a) parent alloy, (b) the WNZ, and (c) the HAZ before corrosion test.

Table 4 – Simulated parameters of the EIS data of parent alloy and weld regions in 0.6 mol L^{-1} with pH = 6.5 at 25 ± 1 °C.

Material/process	R_s (Ω)	C (μF)	R_p (Ω)	$Y_{0(1)}$ (Ω^{-1} S^n)	n_1	R_1 (Ω)	$Y_{0(2)}$ (Ω^{-1} S^n)	n_2	R_1 (Ω)
Parent alloy	7.07	7.75	24.31	4.95	0.84	1256	1.54	0.99	151.1
FSLW joint-WNZ	6.51	7.25	18.83	6.47	0.85	1215	–	0.98	104.6
FSLW joint-HAZ	4.90	5.96	17.78	8.42	0.89	942.3	–	0.88	74.1

denser due to the constants of the two layers. In addition, it can be found that these layers have good adhesion together. As seen in Table 4, the resistance values for the parent alloy were higher than those for the weld regions. This suggests that the weld regions have a lower corrosion resistance. Indeed, as it can be seen from Nyquist plot in Fig. 3, the parent alloy has higher impedance than that of the WNZ and HAZ because the semicircle radios of Nyquist plot follows: PA > WNZ > HAZ in the same solution. The low frequency impedance indicates the corrosion resistance. Hence, higher impedance value at low frequency indicates better corrosion resistance. Thus, the weld regions exhibit lower resistance compared to the parent alloy. Based on Bode magnitude diagram, the higher impedance was obtained for parent alloy compared to the WNZ, and the HAZ. This is also in good agreement with previous results from the Nyquist plot. It is known that the nobler electrochemical behavior is related to modulus of impedance |Z|. Moreover, although the Bode plots have not clearly permitted to conclude the better electrochemical behavior for these examined samples, the aforementioned Nyquist plots induced that PA samples better than both the WNZ and HAZ, as previously demonstrated. The results obtained from EIS measurements suggest that the weld regions have lower corrosion resistance than the parent alloy. In this case, the HAZ has the lowest corrosion resistance.

3.2. *Microstructural analysis before corrosion*

The SEM image of parent alloy and various weld regions of lap welded joint region are shown in Fig. 3. The bright and dark regions represent the phases of Fe and Si elements precipitated from the solid solution of Al alloy, respectively. Accordingly, it can be seen that none of the constituent precipitates including Fe-rich (bright regions) and Si-rich (dark regions) were dissolved, and remained in the Al matrix during FSLW. This can be attributed to the fact that although the WNZ experienced the peak temperature around 550 °C in FSLW, none of the Fe-rich and Si-rich precipitates were dissolved totally due to having the highest melting points temperature [12,21]. The dimension of constituent particles in the lap welded joint is smaller than that in the parent alloy, and their distribution is wider than that in the parent alloy. In this case, the stirring, which is related to the rotation of the tool, can create different size and distribution of constituent precipitates in welded joints. The stirring can break down the constituent particles and distribute them into the Al matrix. In this respect, these precipitates cause an increase in the strength of parent alloy. This means that they act as strengthening precipitates in the parent alloy and various weld regions. Moreover, the strengthening precipitates can affect localized corrosion of parent alloy and various weld regions in corrosive environments. It can be supposed that the localized corrosion

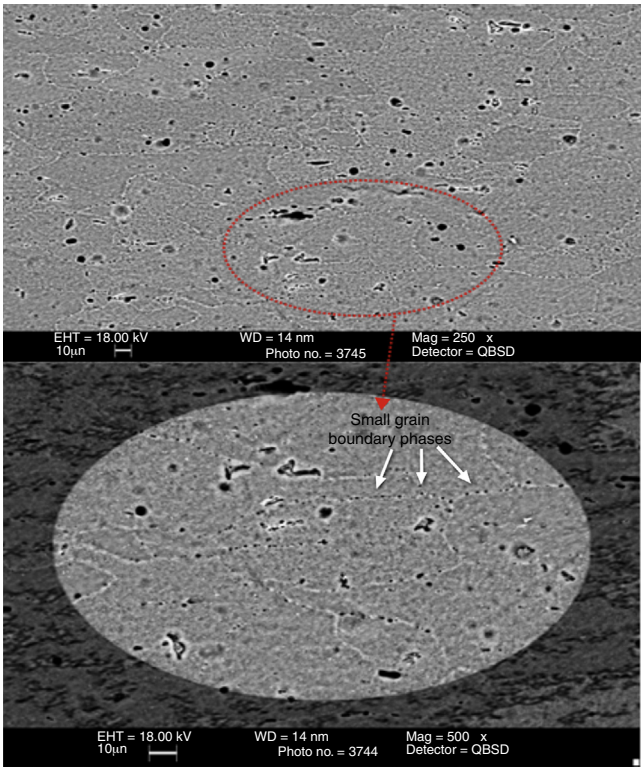

Fig. 4 – SEM micrograph of small grain boundary phases in parent alloy (PA) before corrosion test.

resistance of the welded joint is more than that in the parent alloy. Indeed, the parent alloy zone shows semi-round-shaped precipitate particles as an intergranular segregation in the grain boundaries as reported in Fig. 4. This means that intergranular segregation is prominent in this area. These semi-round-shaped particles are rich by Si phases (Fig. 5).

The friction stir welding creates the microstructural evolution of the increased constituent particles in the HAZ and WNZ of AA6061-T6 Al alloy. The HAZ has a finer grain compared to the parent alloy zone. The size of precipitates in this area was smaller than that in the parent alloy, and the distribution of constituent particles was also wider than that in the parent alloy. The fine constituent particles can be seen in the WNZ. It is important to note that the dimension and distribution of constituent particles in the HAZ area are more than those in the weld nugget zone (WNZ). In this region, similar to the parent alloy, some grain boundary phases can also be seen in the grain boundaries. Thus, coarse intragranular precipitates and grain boundary phases cause the occurrence of the intergranular or intersubgranular corrosion. Electrochemically nobler behavior constituted by both the Si-rich and Fe-rich phases associated with anode/cathode area ratio (i.e. between nobler

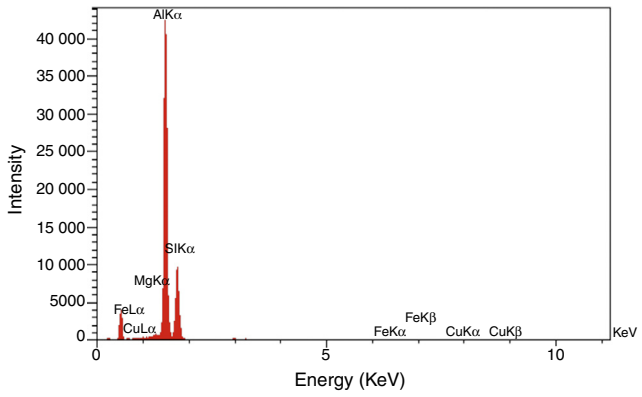

Fig. 5 – The EDS analysis of small grain boundary phases in parent alloy (PA).

Si and Fe-rich phases and grain Al-based matrix) and high deformation level into a grain refined microstructure array conducts to corrosion response of these examined samples. The EDS analysis results of constituent precipitates are shown in Table 5. According to this Table, it is obvious that the value of average composition (wt%) of Si-rich and Fe-rich particles are decreasing from parent alloy to weld nugget zone (WNZ) for welded joints, but it is important to note that the values of Si-rich and Fe-rich particle composition in the welded joint are lower than those in the parent alloy.

3.3. *Microstructural analysis after corrosion*

Fig. 6 reports a magnification of the surfaces of the parent alloy, the WNZ and HAZ after the cyclic polarization test. A careful observation of these picture reveals that lap welded joints showing marked intergranular attack (pointed as cracks) exhibit an E_{ptp} transition in the cyclic polarization plot of Fig. 1. Several authors reported that pitting and intergranular corrosion were often encountered together in aluminum alloy [22–25]. The intergranular corrosion nucleates on pit walls and spreads from them. The variation in pit shape mainly depends on the microstructure of parent alloy and welding conditions. It has to be noted that the SEM micrographs of the corroded surfaces of the parent alloy and welded lap joints after cyclic polarization experiments strongly support the electrochemical measurements feature. In this case, these micrographs clearly show that the damages caused by these types of corrosion are accentuated in near-natural solution, suggesting that the corrosion resistance of the welded joints in each region

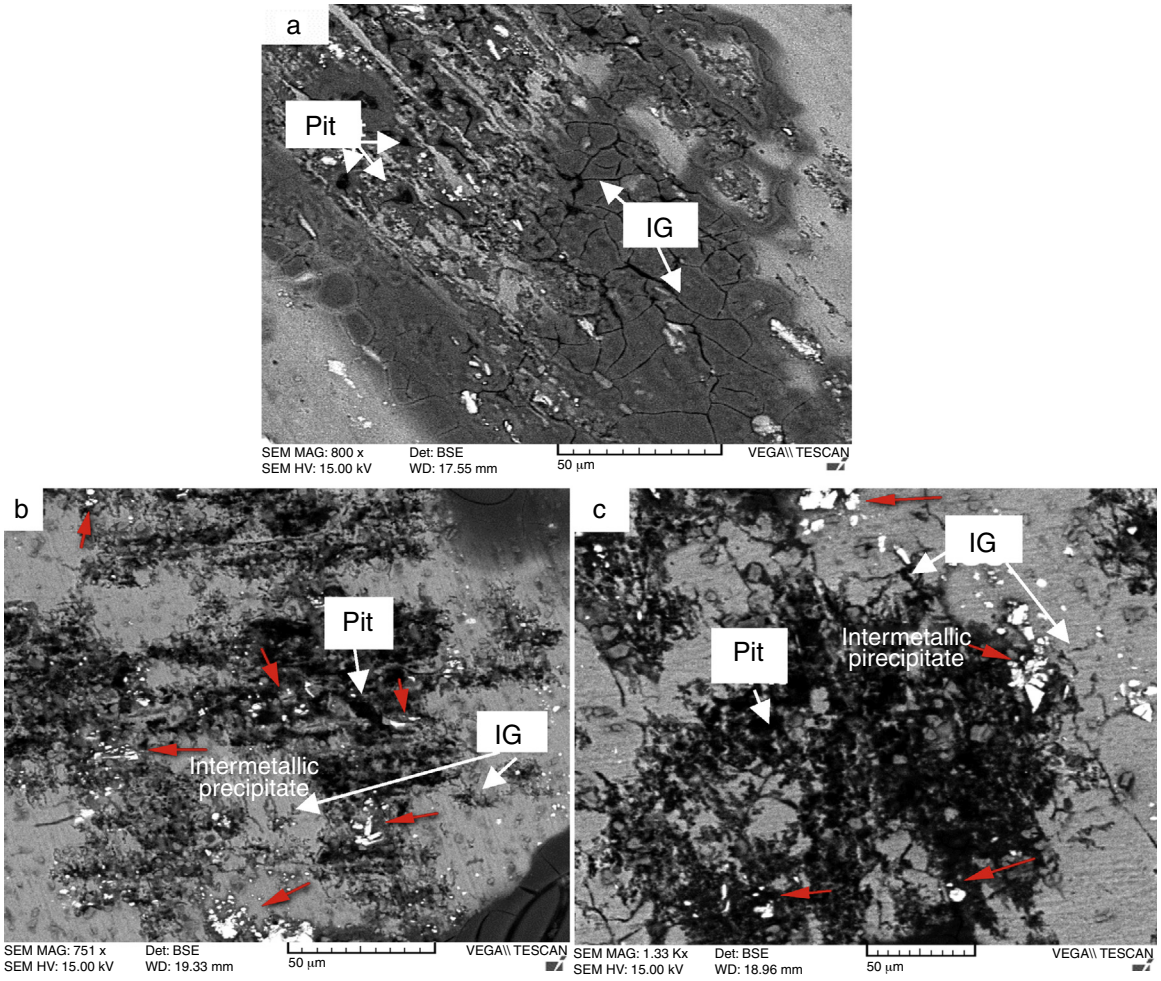

Fig. 6 – BSE images of (a) parent alloy (b) the WNZ, and (c) the HAZ surfaces after pitting scans in 0.6 mol L^{-1} with pH = 6.5 at 30 °C.

Table 5 – EDS analysis (wt%) of different intermetallic precipitates highlighted in weld regions and parent alloy shown in Fig. 3.

Location	Point	Composition (wt%)					
		Al	Mg	Si	Fe	Cu	Cr
Parent alloy	A	90.46	0.66	1.75	6.8	0.21	0.12
	B	89.58	0.18	9.83	0.41	–	–
FSLW-HAZ	C	90.24	0.85	1.86	6.41	0.28	0.36
	D	89.98	0.16	9.31	0.55	–	–
FSLW-WNZ	E	91.69	0.76	1.31	5.8	0.18	0.26
	F	90.99	0.11	8.50	0.4	–	–

was lower than the parent alloy. It is to be noted that pitting attacks were observed on the WNZ and HAZ (Fig. 6). It can be seen that the density and size of pits in the WNZ are lower in comparison to those in the HAZ region. Hence, the HAZ region showed poor resistance to corrosion.

It can further be seen in Fig. 6 that the same constituent intermetallic particle is in the pitting areas. Many studies have proved that intermetallic particles affect the corrosion behavior of Al alloys [17–20]. It has recently been reported that the morphology of the intermetallic particles (i.e. spheroids, fiber-like or plate-like) and its cathodic/anodic area ratio are intimately associated with the resulting corrosion behavior of a number of alloys. This morphology is strongly affected by the applied cooling rate during solidification [26,27]. Thus, the increased constituent particles cause the aggravation of pitting and cracking in the WNZ and HAZ. According to Fig. 6 for parent alloy, it is observed that a film, which is generated by corrosion products, shows cracks that are not compact and are almost heterogeneous. These cracks could be related to the intergranular corrosion in the parent alloy after the corrosion test. As for the friction stir lap welds, the weld regions, especially the HAZ, suffers more severe pitting compared with the parent alloy. Many small intergranular attacks are associated with the corroded surface of the HAZ. It is to be noted that the galvanic corrosion existed between the weld regions and the constituent particles, which have differences in chemical composition and microstructure. In this case, it is supposed that the cathodic process at the constituent particles inducing to an alkalization [28,29] that in turn leads to the dissolution of Al matrix and also may be the surface film resulting in the porous surface layer.

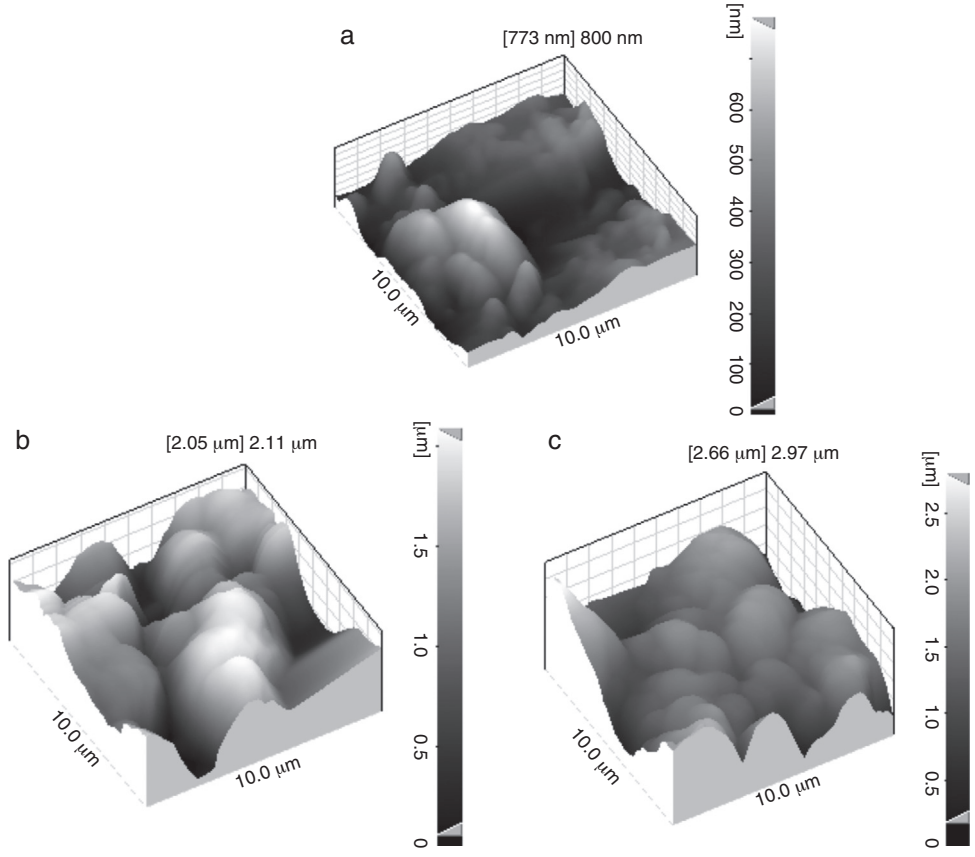

Fig. 7 – Three-dimensional AFM images of the samples surface after pitting scan: (a) parent alloy, (b) WNZ, and (c) HAZ regions for FSLW.

It seems that the enhanced corrosion in the weld regions of welded lap joints is attributed to the increased constituent particles in the weld regions. Corrosion potential of an intermetallic particle is not the same as the Al matrix phase. This variation in potential creates the formation of a galvanic cell [30]. The potential difference between intermetallic particles and Al matrix causes the formation of corrosion cells. It can be noticed that higher amounts of intermetallic particles lead to more cathodic reaction. In this regard, increase in constituent particles increases the sites for galvanic coupling, and hence, decreases the corrosion resistance [6]. The constituent particles are cathodic to the Al matrix and lead to localized corrosion of the latter Al matrix. Localized galvanic corrosion increases between the constituent particles and Al matrix. The enhanced hydrogen evolution also exists in the cathodic constituent particles in the weld regions [30].

Fig. 7(a)–(c) displays three-dimensional images of the parent alloy sample surface as well as those for the WNZ and the HAZ after the corrosion test. This figure presents a good amount of quantitative data related to the corrosion attacks occurring on the sample surfaces. Compared to the parent alloy, the amount of corrosion attacks increased significantly from the WNZ to the HAZ for FSLW and the intensity of corrosion attacks on the surfaces of the FSLW samples is greater than that of the parent alloy samples.

4. Conclusions

- Friction stir welding enhanced the corrosion susceptibility of AA6061-T6 aluminum alloy, so that in the weld regions, intergranular attack associated with pitting corrosion was observed.
- Although the parent alloy and the weld regions showed the same corrosion attacks, the HAZ region exhibited intensive corrosion attack as opposed to the WNZ and the parent alloy.
- The increased intermetallic constituent particles during welding process increased the galvanic corrosion coupling, and hence decreased the corrosion resistance of weld regions.
- SEM and AFM images showed that the susceptibility to corrosion attacks in the HAZ for FSLW is higher than that at the WNZ, as opposed to the parent alloy.

Conflicts of interest

The authors declare no conflicts of interest.

Acknowledgments

The authors wish to place sincere special thanks to Dr. Mohd Khairol Anuar Mohd Ariffin Head of Department of Mechanical and Manufacturing, Faculty of Engineering, Universiti Putra Malaysia (UPM) for their technical supports. Also, the authors are grateful to Prof. Muna K. Abbas from Department of Production Engineering and Metallurgy University of Technology, Baghdad and to Prof. Abdul Razak Daud from the School of Applied Physics, Faculty of Science and Technology, University Kebangsaan Malaysia (UKM) for their help and guidance to do this research.

REFERENCES

[1] Nikseresht Z, Karimzadeh F, Golozar MA, Heidarbeigy M. Effect of heat treatment on microstructure and corrosion behaviour of Al6061 alloy weldment. Mater Des 2010;31:2643–8.
[2] Ambat R, Davenport AJ, Scamans MG, Afseth A. Effect of iron-containing intermetallic particles on the corrosion behaviour of aluminium. Corros Sci 2006;48: 3455–71.
[3] Guillaumin V, Mankowski G. Localized corrosion of 6056 T6 aluminium alloy in chloride media. Corros Sci 2000;42:105–25.
[4] Abbas MK. Effect of friction stir welding on the microstructure and corrosion behavior of aluminum alloy AA6061-T651. In: Proceedings of the 2nd regional conference for engineering sciences. 2010.
[5] Birbilis N, Buchheit RG. Electrochemical characteristics of intermetallic phases in aluminium alloys an experimental survey and discussion. J Electrochem Soc 2005;152:B140–51.
[6] El-Menshawy K, El-Sayed A, El-Bedawy ME, Ahmed HA, El-Raghy SM. Effect of aging time at low aging temperatures on the corrosion of aluminium alloy 6061. Corros Sci 2012;54:167–73.
[7] Fahimpour V, Sadrnezhaad SK, Karimzadeh F. Corrosion behaviour of aluminium 6061 alloy joined by friction stir welding and gas tungsten arc welding methods. Mater Des 2012;39:329–33.
[8] Weifeng X, Jnhe L, Hongqiang Z. Pitting corrosion of friction stir welded aluminium alloy thick plate in alkaline chloride solution. Electrochim Acta 2010;55:2918–23.
[9] Paglia CS, Buchheit RG. A look in the corrosion of aluminium alloy friction stir welds. Scripta Mater 2008;58:383–7.
[10] Astarita A, Squillace A, Scala A, Prisco A. On the critical technology issue of friction stir welding T-joint of dissimilar aluminium alloys. J Mater Eng Perform 2012;21: 1763–71.
[11] Ciliberto S, Astarita A, Squillace A. FSW of T joints overlap configuration: process optimization in joining dissimilar aluminium alloys for the aeronautic application. Surf Interface Anal 2013;45:1631–7.
[12] Lumsden JB, Mahoney MW, Rhodes CG, Pollock GA. Corrosion behaviour of friction-stir-welded AA7050-T7651. Corrosion 2003;59:212–9.
[13] Astarita A, Bitondo C, Squillace A, Arentani E, Bellucci F. Stress corrosion cracking behaviour of conventional and innovative aluminium alloys for aeronautic applications. Surf Interface Anal 2013;45:1610–8.
[14] Lumsden JB, Mahoney MW, Rhodes CG, Pollock GA. Intergranular corrosion following friction stir welding of aluminium alloy 7075-T651. Corrosion 1999;55:1127–35.
[15] Hu W, Meletis EI. Corrosion and environment-assisted cracking behaviour of friction stir welded Al2195 and Al2219 alloys. Mater Sci Forum 2000;331–337:1683–8.
[16] Frankel GS, Xia Z. Localized corrosion and stress corrosion cracking resistance of friction stir welded aluminium alloy 5454. Corrosion 1999;55:139–50.
[17] Corral J, Trillo EA, Li Y, Murr LE. Corrosion of friction stir welded aluminium alloys 2024 and 2195. J Mater Sci Lett 2000;19:2117–22.
[18] Zucchi F, Trabanelli G, Grassi V. Pitting and stress corrosion cracking resistance of friction stir welded AA5083. Mater Corros 2001;52:853–9.

[19] Trueba M, Trasatti SP. Study of Al alloy corrosion in neutral NaCl by the pitting scan technique. Mater Chem Phys 2010;121:523–33.
[20] Zaid B, Saidi D, Benzaid A, Hadji S. Effects of pH and chloride concentration on pitting corrosion of AA6061 aluminum alloy. Corros Sci 2008;50:1841–7.
[21] Birbillis N, Buchheit RG. Investigation and discussion of characteristics for intermetallic phases common to aluminum alloys as a function of solution pH. J Electrochem Soc 2008;155:C117–26.
[22] Niranjani VL, Kumar KCH, Subramanja SS. Development of high strength Al–Mg–Si AA6061 alloy through cold rolling and ageing. Mater Sci Eng A 2009;515:169–74.
[23] Braun R. Effect of thermal exposure on the microstructure, tensile properties and the corrosion behavior of 6061 aluminum alloy sheet. Mater Corros 2005;56:159–65.
[24] Vargel C, Jacques M, Schmidt MP. Corrosion of aluminum. Elsevier; 2004. p. 125.
[25] Amini M, Kazemzade F, Moayed MH. An approach to predict galvanic corrosion using identical couple electrodes; investigation of weld zone and parent alloy in AA6xxx welded through FSW technique. In: Proceedings of Iran international aluminum conference (IIAC 2009). 2009.
[26] Osorio WR, Garcia LR, Peixoto LC, Garcia A. Electrochemical behavior of a lead-free snag solder alloy affected by the microstructure array. Mater Des 2011;32:4763–72.
[27] Osorio WR, Freire CM, Caram R, Garcia A. The role of Cu-based intermetallics on the pitting corrosion behavior of Sn–Cu, Ti–Cu and Al–Cu alloys. Electrochim Acta 2012;77:189–97.
[28] Ezuber H, El-Houd A, El-Shawesh F. A study on the corrosion behaviour of aluminium alloys in seawater. Mater Des 2008;29:801–5.
[29] Park JO, Paik CH, Huang YH, Alkire RC. Influence of Fe-rich intermetallic inclusions on pit initiation on aluminium alloys in aerated NaCl. J Electrochem Soc 1999;146:517–23.
[30] Zhang D, Li J, Joo HG, Lee KY. Corrosion properties of Nd:YAG Laser–GMA hybrid welded AA6061 Al alloy and its microstructure. Corros Sci 2009;51:13991404.